ELSEVIER

Materials Science and Engineering A 447 (2007) 51–57

MATERIALS SCIENCE & ENGINEERING A

www.elsevier.com/locate/msea

Molecular dynamics study of the stress–strain behavior of carbon-nanotube reinforced Epon 862 composites

R. Zhu [a], E. Pan [a,*], A.K. Roy [b]

[a] *Department of Civil Engineering, University of Akron, Akron, OH 44325, USA*
[b] *Materials and Manufacturing Directorate, Air Force Research Laboratory, AFRL/MLBC, Wright-Patterson Air Force Base, OH 45433, USA*

Received 9 March 2006; received in revised form 2 August 2006; accepted 20 October 2006

Abstract

Single-walled carbon nanotubes (CNTs) are used to reinforce epoxy Epon 862 matrix. Three periodic systems – a long CNT-reinforced Epon 862 composite, a short CNT-reinforced Epon 862 composite, and the Epon 862 matrix itself – are studied using the molecular dynamics. The stress–strain relations and the elastic Young's moduli along the longitudinal direction (parallel to CNT) are simulated with the results being also compared to those from the *rule-of-mixture*. Our results show that, with increasing strain in the longitudinal direction, the Young's modulus of CNT increases whilst that of the Epon 862 composite or matrix decreases. Furthermore, a long CNT can greatly improve the Young's modulus of the Epon 862 composite (about 10 times stiffer), which is also consistent with the prediction based on the *rule-of-mixture* at low strain level. Even a short CNT can also enhance the Young's modulus of the Epon 862 composite, with an increment of 20% being observed as compared to that of the Epon 862 matrix.

Keywords: Carbon nanotube; Epon 862; Nanocomposite; Molecular dynamics; Stress–strain curve

1. Introduction

In recent years, nanoparticle reinforced polymer composites have led to intensive research in the field of nanocomposites. Carbon nanotubes (CNTs) [1,2] have shown their high potential in improving the material properties of polymers. Besides the improved electrical conductivity [3–6] and thermal conductivity [7,8], the improvement of mechanical properties is also of special interest. This originates from recent observations that CNTs are exceptionally stiff, strong, and tough [9,10]. By combining CNTs with brittle materials one can impart some of the attractive mechanical properties of the CNTs to the resulting composites, thus making CNT an excellent candidate as reinforcement for polymeric materials.

While some studies on CNT composite materials were carried out experimentally [11–22], the reinforcement theory is still not clear so far. In particular, during the mixture process of CNT-reinforced composites, some of the CNTs might be destroyed and the alignment of CNTs cannot be exactly straight. As such, analytical/numerical studies on the effective stiffness of the composites would be very helpful in understanding the reinforcement. Computer simulations are increasingly used to guide experimentalists in interpreting their experimental results and even to replace some of the laboratory tests. For large systems with hundreds of atoms and more, the molecular dynamics (MD) simulation is an important tool to understand the properties of polymer–CNT composites. In several earlier works, MD simulations have been successfully applied to the prediction of elastic properties of polymer–CNT composites [23–26]. The properties of Epon 862 categorize itself as a thermosetting polymer with highly crossing linked polymer chains that form an irreversible network structure. As a result, this material is very strong due to its tight linkage; unfortunately, however, it is relatively brittle with low stiffness. The excellent mechanical properties of CNTs, therefore, should be helpful in taking care of the inherent brittleness and low stiffness of Epon 862 matrix.

The purpose of this work is to utilize the MD method to simulate the stress–strain curves for CNT-reinforced Epon 862 composites. The simulated stress–strain curves are then used to

* Corresponding author. Fax: +1 330 972 6020.
E-mail address: pan2@uakron.edu (E. Pan).

0921-5093/$ – see front matter © 2006 Elsevier B.V. All rights reserved.
doi:10.1016/j.msea.2006.10.054

predict the corresponding effective Young's moduli in the longitudinal direction. The well-known *rule-of-mixture* is further employed to predict the effective Young's moduli. Three periodic systems are considered, namely, a long CNT-reinforced Epon 862 composite, a short CNT-reinforced Epon 862 composite, and the Epon 862 matrix itself, with the applied strain increasing from 0 to 0.1.

This paper is presented as follows: in Section 2, we discuss the detailed MD simulation process using the software *Cerius 2* developed by Accelrys. The key equations for the system energy and stress–strain relation are also presented. In Section 3, typical numerical results from MD and *rule-of-mixture* are analyzed, and in Section 4, we draw our conclusions.

2. Molecular dynamics simulation

2.1. MD models

Three models, namely, Epon 862 matrix itself, the Epon 862 matrix reinforced with long single-walled CNT(10,10) (Fig. 1a), and Epon 862 matrix reinforced with short single-walled CNT(10,10) (Fig. 1b), are studied. Nanotubes form different types, which can be described by the chiral vector (n, m) in terms of the primitive in-plane lattice vectors of a grapheme sheet [27]. For the given chiral vector (n, m), the diameter of a CNT can be determined using the relationship $d = 0.0783\,\text{nm}\,(n^2 + m^2 + nm)^{1/2}$. For each model, the amorphous cuboid specimen (matrix) with a size of $40.28\,\text{Å}^3 \times 40.28\,\text{Å}^3 \times 61.09\,\text{Å}^3$ is constructed and the periodic boundary condition is applied in all three directions. The long and short CNTs have a length of 61.09 Å and 29.32 Å, respectively. Strain is applied to the specimen by uniformly expanding the length of the simulation cell in the longitudinal CNT direction. To equilibrate the system for the new cell size, the coordinates of the atoms are re-scaled to fit the new geometry. Potential energy minimization and the MD simulation (NVT ensemble) are performed at room temperature. The NVT ensemble is one which is free to exchange energy, but keeps constant number of particles, constant volume and temperature. Therefore, by applying different expansions in the longitudinal direction of the model samples, the stresses at different strains can be simulated successively.

While the MD simulation model for CNT(10,10) is well known, we will also need a computer model for Epon 862. The Epon 862 molecule models are constructed by following the chemical structure of Epon 862 (Fig. 2a) and using a many-body bond-order potential according to Brenner et al. [28,29] for the bonding interaction within this hydrocarbon system (Fig. 2b). The Brenner's reactive empirical bond-order potential is a potential energy function for solid carbon and hydrocarbon molecules. This potential allows for covalent bond breaking and forming with associated changes in atomic hybridization within a classical potential, producing a powerful method for modeling complex chemistry in large many-atom systems. Specifically, the Epon 862 chains are simulated with a molecular-mechanics force field adapted from Ref. [30] and separated by using the SHAKE algorithm, a constraint dynamics method which constrains the bond length within a user-defined tolerance [31]. The van der Waals interfacial interactions among the Epon 862 molecules and between the Epon 862 molecules and the CNTs are modeled using the Lennard–Jones potential [31],

$$U = 4\varepsilon\left(\frac{\sigma^{12}}{r^{12}} - \frac{\sigma^{6}}{r^{6}}\right) \tag{1}$$

where U is the potential energy between a pair of atoms, r the separation distance between the pair of atoms, ε the potential well depth, and σ is the van der Waals separation distance. For interaction between the carbon atoms of the CNT and the Epon 862 molecular units, the Lennard–Jones potential was parameterized with $\varepsilon = 0.4742\,\text{kJ/mol}$ and $\sigma = 0.4280\,\text{nm}$ [30,31]. Lennard–Jones potential is also used to describe the non-bonding interaction among Epon 862 molecules. For these interactions, $\varepsilon = 0.4492\,\text{kJ/mol}$ and $\sigma = 0.3825\,\text{nm}$

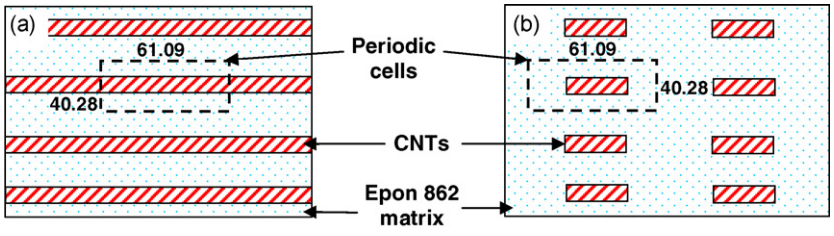

Fig. 1. Schematic arrangement of Epon 862 matrix filled with long (a) and short (b) CNTs.

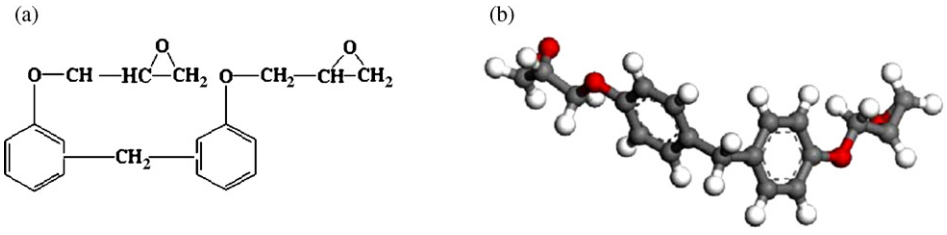

Fig. 2. Epon 862 molecular structure (a) and computer constructed molecules of Epon 862 (b).

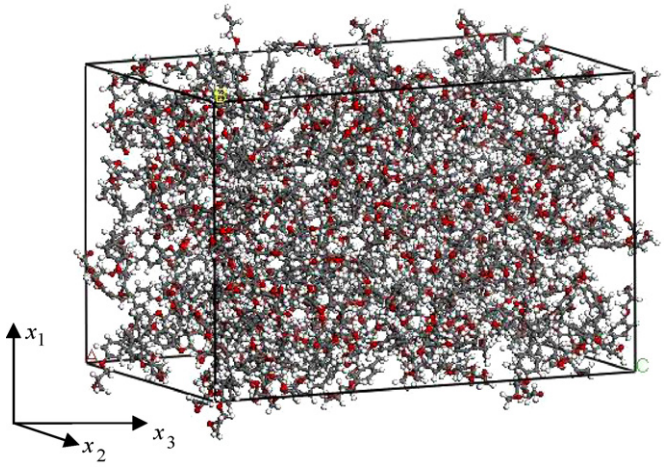

Fig. 3. Computer constructed Epon 862 matrix with the size of $l_1 \times l_2 \times l_3 = 40.28\,\text{Å}^3 \times 40.28\,\text{Å}^3 \times 61.09\,\text{Å}^3$ (the CNT is embedded along the longitudinal x_3-direction as shown in Fig. 4).

[30,31]. Using the constructed Epon 862 molecules and setting the Lennard–Jones non-bonding interaction for Epon 862 molecules, an amorphous Epon 862 matrix with the size of $40.28\,\text{Å}^3 \times 40.28\,\text{Å}^3 \times 61.09\,\text{Å}^3$ and density of 1 g/cm^3 is constructed at room temperature. The long-time minimization and NVT dynamic process are then applied to the amorphous Epon 862 matrix in order to obtain a stable Epon 862 matrix (Fig. 3). After that, we insert the long (Fig. 4a) and short (Fig. 4b) CNTs inside the Epon 862 matrix and delete all the molecules inside the CNTs. Again, after long-time minimization and NVT dynamic process, we obtain the stable CNT-reinforced Epon 862 composites. We also remark that the periodic boundary condition is used to replicate the cells in all three directions and that all the simulations are carried out at temperature of 298 K with a 1 fs time step.

2.2. Simulation of stress–strain relationship

A long specimen is under axial loading when the only applied force is along its longitudinal direction. The internal force is normal to the plane of the cross-section and the corresponding stress is described as a normal stress. The stress is obtained by dividing the internal force distributed over the cross-section by the cross-section area, thus it represents the average value of the stress over the cross section. The ratio of the stress to strain, or the slope of the stress–strain curve, is the so-called well-known Young's modulus.

In our MD simulation, totally five increments with 2% each are applied in the longitudinal direction. For each increment of the applied deformation, a uniform strain is applied to the entire specimen. In other words, each increment is accomplished by uniformly expanding the cell in the longitudinal direction and re-scaling the new coordinates of the atoms to fit within the new dimensions. The increment is achieved in two equal steps of 1% each 1 ps (1000 steps) apart. After adding each 2% increment of strain, the system is minimized with 20 ps (20,000 steps) and 10 ps NVT ensemble (10,000 steps). During the minimization and NVT process, the atoms are allowed to equilibrate within the new MD cell dimensions.

Stress is an important concept in characterizing the mechanical behavior of condensed matters. For a volume element within a stressed body, we can distinguish two types of forces: those acting directly in the interior of the element and those exerted upon the surface of the element by the surrounding material. At the continuum level, the stress tensor, σ_{ij}, is defined as the change in the internal energy (in the thermodynamic sense) with respect to the strain tensor ε_{ij} per unit volume [32]

$$\sigma_{ij} = \frac{1}{V}\left(\frac{\partial E}{\partial \varepsilon_{ij}}\right)_s \tag{2}$$

where V is the volume of the solid, E the total internal energy, and the subscript s denotes constant entropy. At the atomistic level, the total internal energy is the summation of the kinetic energy (E_K) due to the dynamic motion of molecules, the potential energy (E_P) associated with the deformation, and the electric energy of atoms within molecules. It includes the energy in all the chemical bonds and the energy of the free and conductive electrons in the matter, but not the translational or rotational kinetic energy of the body as a whole. Furthermore, in general, the total internal energy E given in Eq. (2) can also be expressed

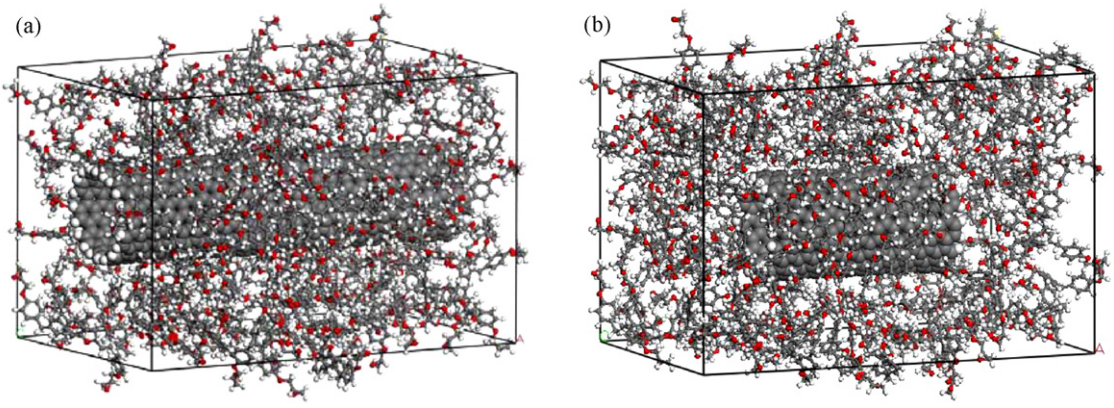

Fig. 4. Long (a) and short (b) CNT(10,10)-reinforced Epon 862 matrix ($40.28\,\text{Å}^3 \times 40.28\,\text{Å}^3 \times 61.09\,\text{Å}^3$). Lengths of the long and short CNTs are 61.09 Å and 29.32 Å, respectively.

as the summation of the energies of the individual atoms, E^α, that compose the solid:

$$E = \sum_\alpha (E^\alpha) = \sum_\alpha (E_K^\alpha + E_P^\alpha) = \frac{1}{2} M^\alpha (v^\alpha)^2 + \Phi^\alpha(\boldsymbol{r}) \quad (3)$$

where α is the atom index, E_K^α the kinetic energy, E_P^α the potential energy, M^α the mass, v^α the magnitude of the velocity, and $\Phi^\alpha(\boldsymbol{r})$ is the potential energy at the atom location $\boldsymbol{r}$. In the mathematical formulation of quantum mechanics, the physical state of a system may be characterized as a vector in an abstract Hilbert space (or, in the case of ensembles, as a countable sequence of vectors weighted by probabilities). Physically observable quantities are described by self-adjoint operators acting on these vectors. The quantum Hamiltonian H is the observable corresponding to the total energy of the system. Mathematically speaking, it is a densely defined self-adjoint operator. As used by others [33,34], using a Hamiltonian based on these individual energy contributions, it was shown that the stress contribution, σ_{ij}, for a given atom α is

$$\sigma_{ij}^\alpha = -\frac{1}{V^\alpha}\left(M^\alpha v_i^\alpha v_j^\alpha + \sum_\beta F_i^{\alpha\beta} r_j^{\alpha\beta}\right) \quad (4)$$

where V^α is the atomic volume of atom α, v_i^α the i-component of the velocity of atom α, $F_i^{\alpha\beta}$ the i-component of the force between atoms α and β obtainable from the derivative of the potential $\Phi(\boldsymbol{r})$, and $r_j^{\alpha\beta}$ is the j-component of the separation of atoms α and β [33,34]. The stresses used to generate the stress–strain curves for the CNT composites are the average atomic stresses for the volume of the model. Therefore, the stress components of each model are calculated for each strain increment by taking the summation of Eq. (4) over all the atoms. The results will then be further averaged over the time via the MD simulation.

2.3. Rule-of-mixture

For a nanocomposite under uniaxial loading, the dependence of the elastic modulus on the long CNT volume fraction can be estimated by the *rule-of-mixture* [35]. The longitudinal elastic modulus, Y_3, of the composite cell with long CNTs under constant strain condition is simply expressed as

$$Y_3 = Y_{NT} f_{NT} + Y_m f_m \quad (5)$$

where Y_{NT} and Y_m are the longitudinal elastic moduli of the long CNT and Epon 862 matrix, respectively, f_{NT} and f_m are the volume fractions occupied by the long CNT and Epon 862 matrix, respectively. The volume fractions satisfy

$$f_{NT} + f_m = 1 \quad (6)$$

The long CNT(10,10) used in this work has a radius which is small enough to be treated as a solid beam [36]. Therefore, its volume fraction, f_{NT}, including the entire CNT cross-section, can be approximated as

$$f_{NT} = \frac{\pi(R_{NT} + (h_{eq}/2))^2}{A_{cell}} \quad (7)$$

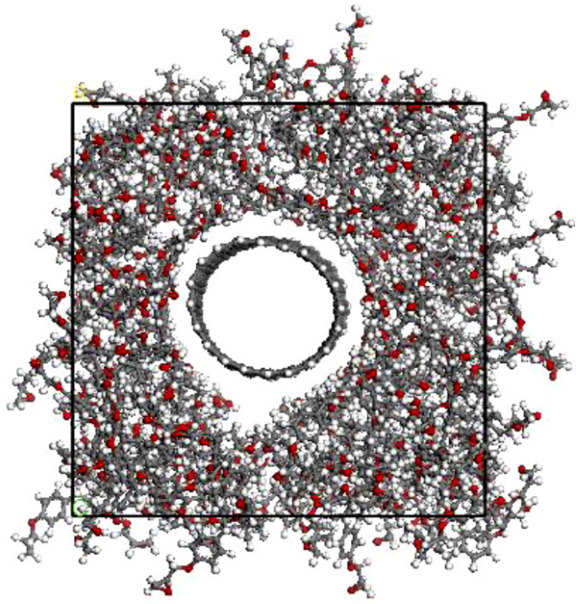

Fig. 5. Equilibrium van der Waals separation distance between the CNT(10,10) and Epon 862 matrix.

where h_{eq} is the equilibrium van der Waals separation distance between the long CNT and Epon 862 matrix, and A_{cell} is the cross-sectional area of the unit cell. The van der Waals separation distance depends on the interfacial interaction between Epon 862 matrix and long CNT (Fig. 5). In this paper after the MD minimization, the separation distance is found to be about 4.0 Å. Consequently, the volume fractions of the long CNT (f_{NT}) and matrix (f_m) are found to be 14.94% and 85.06%, respectively.

3. Numerical results

The MD simulated stress–strain curves for CNT(10,10), long CNT-reinforced Epon 862 composite, short CNT-reinforced Epon 862 composite, and Epon 862 matrix are shown in Fig. 6.

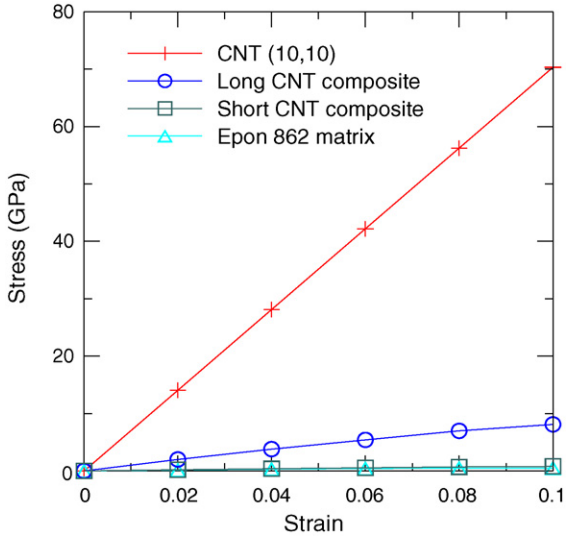

Fig. 6. MD simulated stress–strain curves for CNT(10,10), long and short CNT-reinforced composites, and Epon 862 matrix.

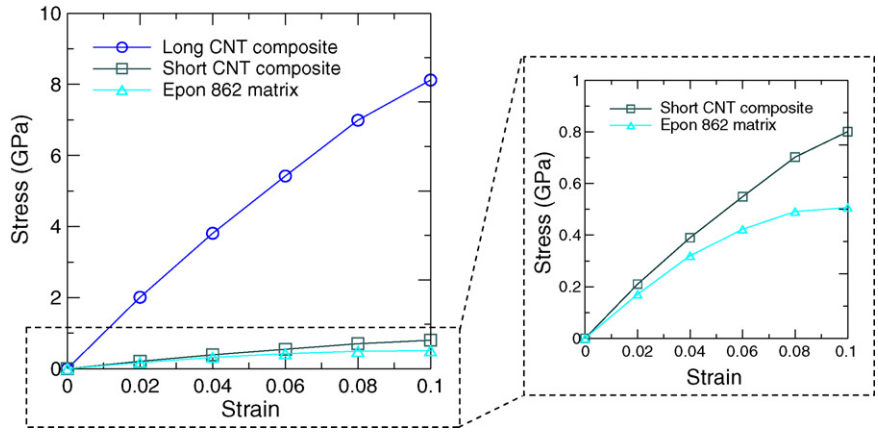

Fig. 7. MD simulated stress–strain curves for CNT-reinforced Epon 862 composites and Epon 862 matrix.

As expected, under the same strain, the stress in the CNT is much larger than those in either the Epon 862 composite or matrix. Therefore, in Fig. 7 we show the MD simulated stress–strain curves for the corresponding long and short CNT-reinforced composites and the matrix only. It is observed from Fig. 7 that the long CNT can substantially enhance the composite stiffness (Fig. 7). Even the short CNT could also improve the corresponding composite stiffness although not as significant as that in the long CNT-reinforced composite (Fig. 7). The stress–strain curves of the long CNT-reinforced composite based on the MD simulation and *rule-of-mixture* are presented in Fig. 8 for comparison. It is observed from Fig. 8 that at low strain level, the results from both approaches are close to each other, although the *rule-of-mixture* always predicts a larger stress than that based on the MD. A large stiffness in the effective property from the *rule-of-mixture* is perhaps due to the fact that in the *rule-of-mixture*, the interface between the CNT and matrix is assumed to be perfectly (mechanically) bonded, whilst the interaction between these two materials could be weak as modeled by the Lennard–Jones potential in the MD. We further remark that, in our MD model, the strain level at the high end (say >0.06) could be already in the plastic deformation domain for the matrix (e.g., [37]).

Using the stress–strain curves obtained, we can also find the effective Young's moduli for these materials. The Young's moduli of CNT(10,10) and Epon 862 matrix are plotted in Fig. 9 as functions of the strain level. It is clear that the Young's modulus of CNT(10,10) increases with increasing strain whilst that of Epon 862 composite or matrix decreases with increasing strain, with the latter being consistent with recent result on CNT reinforcement nanocomposite [38,39].

In Fig. 10, the MD simulated Young's moduli are presented for the long and short CNT-reinforced composites and Epon 862 matrix only. Again, it is noted that the Young's moduli of long and short CNT composites and Epon 862 matrix decrease with increasing strain. The most important feature associated with this figure is, however, on the improvement of the stiffness of the composites: while the long CNT can significantly increase the stiffness of the composite (more than 10 times stiffer than the corresponding Epon 862 matrix), the short CNT can also increase the composite Young's modulus as compared to the

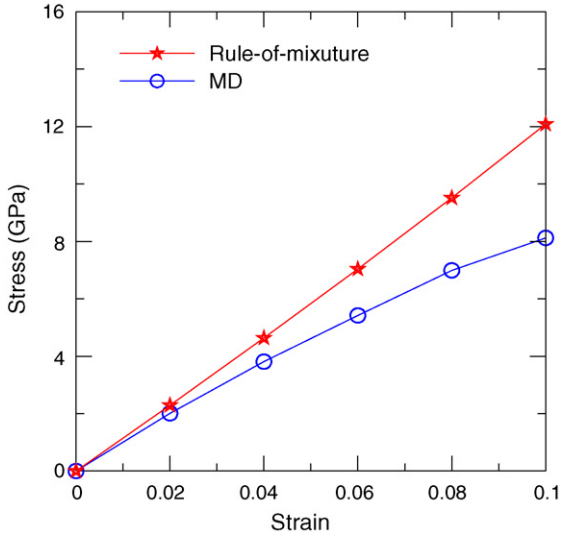

Fig. 8. Stress–strain curves of the long CNT-reinforced composite: MD simulated vs. *rule-of-mixture*.

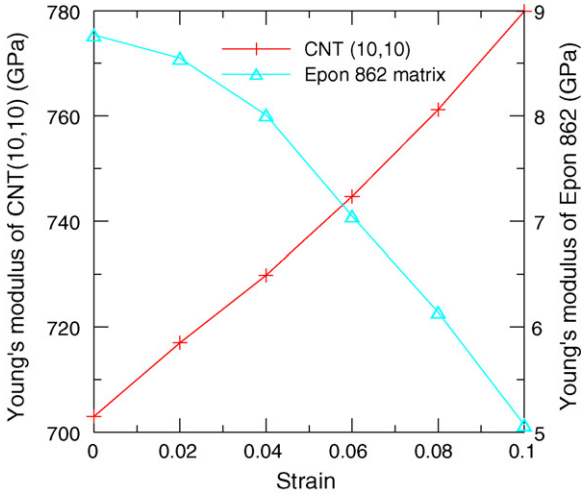

Fig. 9. Variation of MD simulated Young's moduli of CNT(10,10) and Epon 862 matrix with increasing strain.

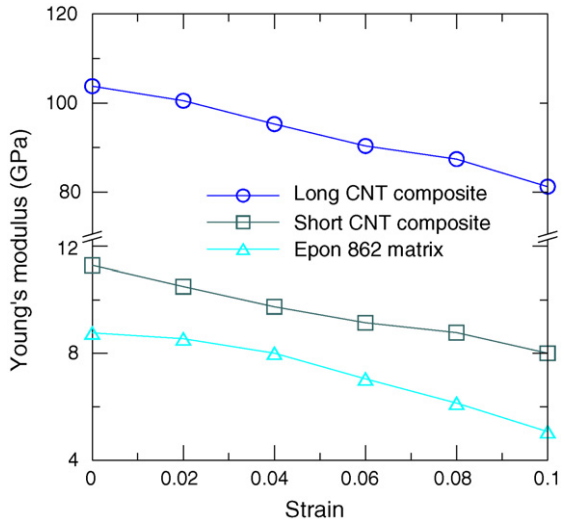

Fig. 10. Variation of MD simulated Young's moduli of long and short CNT-reinforced Epon 862 composites and Epon 862 matrix with increasing strain.

Epon 862 matrix itself. For all the strain levels, an increment of approximately 2 GPa in the Young's modulus can be observed for short CNT-reinforced composites in comparison with that of the Epon 862 matrix, corresponding to a 20% increase in the stiffness.

4. Concluding remarks

Molecular dynamics simulations are utilized to study the stress–strain behavior of the CNT(10,10)-reinforced Epon 862 composites. The three model systems are: a long CNT-reinforced composite, a short CNT-reinforced composite, and the Epon 862 matrix itself. Our MD simulated results indicate clearly that, unlike the pure CNT, the Young's moduli (slopes of the stress–strain curves) of the reinforced composites or the Epon 862 matrix itself generally decrease with increasing strain levels (from 0 to 0.1). Most importantly, however, the MD results show that at any given strain level, the long CNT-reinforced Epon 862 composite can be at least 10 times stiffer than the pure Epon 862 matrix. Even for the short CNT-reinforced Epon 862 composite, its effective Young's modulus can be also increased by roughly 20% as compared to the Epon 862 matrix. We remark that the large difference in the effective Young's moduli between the long and short CNT-reinforced Epon 862 composites is obviously associated to the difference in the CNT volume fractions between these two reinforcements. Furthermore, a long CNT can achieve a full stress transfer from the matrix to CNT, as has been observed by others.

For the long CNT-reinforced Epon 862 composite, we have also compared the MD simulated stress–strain relation to that predicted based on the simple *rule-of-mixture*. While the two curves are very close to each other at low strain level, the curve from *rule-of-mixture* is always above the one from MD, indicating that the perfect interface condition used in the *rule-of-mixture* needs to be modified to accommodate the real imperfect interface behaviors (such as the cohesive-zone model).

Acknowledgments

The authors would like to thank one of the reviewers for his/her constructive comment/suggestion, which have been incorporated into the revised version. The first author (RZ) likes to thank Mr. F. Pan at The School of Chemical Engineering and Technology of Tianjin University for helpful discussion. The second author (EP) is grateful for the Air Force 2005 Summer Faculty Fellowship. This work was also supported in part by AFRL.

References

[1] S. Iijima, Nature 354 (1991) 56–58.
[2] E.T. Thostenson, Z. Ren, T.W. Chou, Compos. Sci. Technol. 61 (2001) 1899–1912.
[3] M. Foygel, R.D. Morris, D. Anez, S. French, V.L. Sobolev, Phys. Rev. B 71 (2005) 104201.
[4] C.A. Martin, J.K.W. Sandler, M.S.P. Shaffer, M.K. Schwarz, W. Bauhofer, K. Schulte, A.H. Windle, Compos. Sci. Technol. 64 (2004) 2309–2316.
[5] J.K.W. Sandler, J.E. Kirk, I.A. Kinloch, M.S.P. Shaffer, A.H. Windle, Polymer 44 (2003) 5893–5899.
[6] Z. Ounaies, C. Park, K.E. Wise, E.J. Siochi, J.S. Harrison, Compos. Sci. Technol. 63 (2003) 1637–1646.
[7] H.M. Duong, D.V. Papavassiliou, L.L. Lee, K.J. Mullen, Appl. Phys. Lett. 87 (2005) 13101.
[8] M.B. Bryning, D.E. Milkie, M.F. Islam, J.M. Kikkawa, A.G. Yodh, Appl. Phys. Lett. 87 (2005) 161909.
[9] M.F. Yu, O. Lourie, M.J. Dyer, K. Moloni, T.F. Kelly, R.S. Ruoff, Science 287 (2000) 637–640.
[10] M.F. Yu, B.S. Files, S. Arepalli, R.S. Ruoff, Phys. Rev. Lett. 84 (2000) 5552–5555.
[11] C.J. Frizzell, M. in het Panhuis, D.H. Coutinho, K.J. Balkus Jr., A.I. Minett, W.J. Blau, J.N. Coleman, Phys. Rev. B 72 (2005) 245420.
[12] H. Ye, H. Lam, N. Titchenal, Y. Gogotsi, F. Ko, Appl. Phys. Lett. 85 (2004) 1775–1777.
[13] P.M. Ajayan, L.S. Schadler, S.C. Giannaris, A. Rubio, Adv. Mater. 12 (2000) 750–753.
[14] R. Haggemueller, H.H. Gommas, A. Rinzler, J.E. Fischer, K.I. Winey, Chem. Phys. Lett. 330 (2000) 219–225.
[15] D. Qian, E.C. Dickey, R. Andrews, T. Rantell, Appl. Phys. Lett. 76 (2000) 2868–2870.
[16] X. Gong, J. Liu, S. Baskaran, R.D. Voise, J.S. Young, Chem. Mater. 12 (2000) 1049–1052.
[17] C. Bower, R. Rosen, L. Jin, J. Han, O. Zhou, Appl. Phys. Lett. 74 (1999) 3317–3319.
[18] M.L. de la Chapelle, C. Stephan, T.P. Nguyen, S. Lefrant, C. Journet, P. Bernier, E. Munoz, A. Benito, W.K. Maser, M.T. Martinez, G.D. de la Fuente, T. Guillard, G. Flamant, L. Alvarez, D. Laplaze, Synth. Met. 103 (1999) 2510–2512.
[19] Z. Jia, Z. Wang, C. Xu, J. Liang, B. Wei, D. Wu, S. Zhu, Mater. Sci. Eng. A 271 (1999) 395–400.
[20] M.S.P. Schaffer, A.H. Windle, Adv. Mater. 11 (1999) 937–941.
[21] L. Jin, C. Bower, O. Zhou, Appl. Phys. Lett. 73 (1998) 1197–1199.
[22] L.S. Schadler, S.C. Giannaris, P.M. Ajayan, Appl. Phys. Lett. 73 (1998) 3842–3844.
[23] Z. Xia, W.A. Curtin, Phys. Rev. B 69 (2004) 233408.
[24] S.J.V. Frankland, V.M. Harik, G.M. Odegard, D.W. Brenner, T.S. Gates, Compos. Sci. Technol. 63 (2003) 1655–1661.
[25] S.J.V. Frankland, A. Caglar, D.W. Brenner, M. Griebel, J. Phys. Chem. B 106 (2002) 3046–3048.
[26] M. Cadek, J.N. Coleman, V. Barron, Appl. Phys. Lett. 81 (2002) 5123–5125.
[27] M.S. Dresselhaus, G. Dresselhaus, P.C. Eklund, Science of Fullerenes and Carbon Nanotubes, Academic Press, New York, 1996.

[28] D.W. Brenner, Phys. Rev. B 42 (1990) 9458–9471.
[29] D.W. Brenner, O.A. Shenderova, J.A. Harrison, S.J. Stuart, B. Ni, S.B. Sinnott, J. Phys.: Condens. Matter 14 (2002) 783–802.
[30] K. Binder, Monte Carlo and Molecular Dynamics in Polymer Sciences, Oxford University Press, New York, 1995.
[31] M.P. Allen, D.J. Tildesley, Computer Simulation of Liquids, Clarendon Press, Oxford, 1987.
[32] C.Y. Fung, Foundations of Solid Mechanics, Prentice-Hall, Englewood Cliffs (NJ), 1965.
[33] O.H. Nielsen, R.M. Martin, Phys. Rev. B 32 (1985) 3780–3791.
[34] V. Vitek, T. Egami, Phys. Status Solidi B: Basic Res. 144 (1987) 145–156.
[35] S.W. Tsai, Composites Design, Think composites Press, Dayton, OH, 1988.
[36] V.M. Harik, Solid State Commun. 120 (2001) 331–335.
[37] G. Subramanian, M.J. Andrews, Nanotechnology 16 (2005) 836–840.
[38] K.T. Lau, Chem. Phys. Lett. 370 (2003) 399–405.
[39] K.T. Lau, M. Chipara, H.Y. Ling, D. Hui, Compos. Part B: Eng. 35 (2004) 95–101.